

## A MEASUREMENT OF WEAK LENSING BY LARGE SCALE STRUCTURE IN RCS FIELDS

HENK HOEKSTRA<sup>1,2,3</sup>, HOWARD K.C. YEE<sup>2,3,4</sup>, MICHAEL D. GLADDERS<sup>2,3,4</sup>,  
 L. FELIPE BARRIENTOS<sup>4,5</sup>, PATRICK B. HALL<sup>2,3,4,5,6</sup>, AND LEOPOLDO INFANTE<sup>4,5</sup>  
*Draft version February 1, 2008*

## ABSTRACT

We have analysed  $\sim 24$  square degrees of  $R_C$ -band imaging data from the Red-Sequence Cluster Survey (RCS), and measured the excess correlations between galaxy ellipticities on scales ranging from 1 to 30 arcminutes. We have used data from two different telescopes:  $\sim 16.4$  square degrees of CFHT data and  $\sim 7.6$  square degrees of CTIO 4-meter data, distributed over 13 widely separated patches. For the first time, a direct comparison can be made of the lensing signal measured using different instruments, which provides an important test of the weak lensing analysis itself. The measurements obtained from the two telescopes agree well. For the lensing analysis we use galaxies down to a limiting magnitude of  $R_C = 24$ , for which the redshift distribution is known relatively well. This allows us to constrain some cosmological parameters. For the currently favored  $\Lambda$ CDM model ( $\Omega_m = 0.3$ ,  $\Omega_\Lambda = 0.7$ ,  $\Gamma = 0.21$ ) we obtain  $\sigma_8 = 0.81^{+0.14}_{-0.19}$  (95% confidence), in agreement with the results from Van Waerbeke et al. (2001) which used fainter galaxies (and consequently higher redshift galaxies). The good agreement between these two very different weak lensing studies demonstrates that weak lensing is a useful tool in observational cosmology.

*Subject headings:* cosmology: observations – dark matter – gravitational lensing

## 1. INTRODUCTION

Weak gravitational lensing has proven to be a powerful tool for studies of the mass distribution in rich clusters of galaxies (for a review see Mellier 1999). Since the pioneering work by Tyson, Wenk, & Valdes (1990) much progress has been made, and nowadays the weak lensing signals induced by clusters of galaxies at intermediate redshifts can be measured without much difficulty.

The development of advanced techniques to correct for the various observational distortions, such as the anisotropy of the point spread function (PSF), the circularization by the PSF, and the camera induced distortion, has been a crucial step, resulting in well calibrated signals (e.g., Kaiser, Squires, & Broadhurst 1995; Luppino & Kaiser 1997; Hoekstra et al. 1998; Kuijken 1999; Refregier 2001). Another important development in recent years is the advent of mosaic CCD cameras, which enable us to quickly image large portions of the sky.

These advances have made it possible to pursue one of the most difficult measurements in the field of weak lensing: the measurement of the coherent distortions of the images of faint galaxies caused by lensing by intervening large scale structure, the so-called ‘cosmic shear’. The analysis of this lensing signal provides an important direct

measurement of the statistical properties of the large scale mass distribution (e.g., Blandford et al 1991; Kaiser 1992; Bernardeau, van Waerbeke, & Mellier 1997; Schneider et al. 1998).

Compared to many other methods that are used to constrain cosmological parameters, weak lensing has the advantage that no assumptions about the light distribution are required. However, weak lensing in itself cannot constrain all the parameters, because of degeneracies between them. Better constraints can be obtained by comparing weak lensing studies that probe different redshifts (e.g., Hu 1999) or when these data are combined with measurements of the fluctuations of the cosmic microwave background (e.g., Hu & Tegmark 1999).

By now, several groups have reported the detection of an excess correlation between galaxy ellipticities, and have argued that this signal is caused by lensing by large scale structure (e.g., Bacon et al. 2000; Kaiser, Wilson, & Luppino 2000; van Waerbeke et al. 2000; Wittman et al. 2000; Maoli et al. 2001; van Waerbeke et al. 2001). Maoli et al. (2001) combined their own results with published measurements in an attempt to obtain constraints on  $\sigma_8$ , the normalisation of the power spectrum, and  $\Omega_m$ , the matter density of the universe. They found good agreement with studies of cluster abundances. However, the data set studied by Maoli et al. (2001) is very inhomogeneous, which limits the accuracy of such a direct comparison.

After these initial detections, which demonstrated the feasibility of the method, the obvious next step is to obtain large uniform data sets. The first results from such a survey were presented by van Waerbeke et al. (2001), who measured a highly significant lensing signal from 6.5 square degrees of deep imaging data.

In this paper we present the results from our analysis of  $\sim 24$  deg<sup>2</sup> of  $R_C$ -band data from the Red-Sequence Cluster Survey (RCS) (e.g., Gladders & Yee 2000), which is a

<sup>1</sup> CITA, University of Toronto, Toronto, Ontario M5S 3H8, Canada

<sup>2</sup> Department of Astronomy and Astrophysics, University of Toronto, Toronto, Ontario M5S 3H8, Canada

<sup>3</sup> Visiting Astronomer, Canada-France-Hawaii Telescope, which is operated by the National Research Council of Canada, Le Centre National de Recherche Scientifique, and the University of Hawaii

<sup>4</sup> Guest observer at the Cerro Tololo Inter-American Observatory (CTIO), a division of the National Optical Astronomy Observatories, which is operated by the Association of Universities for Research in Astronomy, Inc., under cooperative agreement with the National Science Foundation

<sup>5</sup> Universidad Católica de Chile, Depto. Astronomía y Astrofísica, Avda. Vicuña Mackenna 4860, Casilla 306, Santiago 22, Chile

<sup>6</sup> Princeton University Observatory, Princeton, NJ 08544-1001

100 deg<sup>2</sup> galaxy cluster survey designed to provide a large sample of optically selected clusters of galaxies with redshifts  $0.1 < z < 1.4$ . The data are also useful for a range of lensing studies. For example, Gladders, Yee & Ellingson (2001) presented the first results for one of the strong lensing clusters discovered in the survey, for which follow-up observations are underway.

The weak lensing applications are numerous. The survey imaging data are relatively shallow compared to what is common in weak lensing studies, and as a result the statistical uncertainty in the measurements of individual structures (such as clusters of galaxies) is large. However, thanks to the large survey area, many such structures can be detected, and by stacking the signals, one can study their ensemble averaged mass distribution (e.g., Hoekstra et al. 2001). In addition, follow-up observations will provide detailed information on individual systems.

In this paper we concentrate on the measurement of the weak lensing signal induced by large scale structure (cosmic shear). A study of galaxy biasing, based on some of these data, is presented in Hoekstra, Yee, & Gladders (2001), and a study of the properties of galaxy halos is currently underway.

Compared to other cosmic shear studies, the RCS data are shallow, and consequently the signal at a given scale is much lower, as is the signal-to-noise ratio. However, measuring the weak lensing signal from a shallow survey also has several advantages. Down to a limiting magnitude of  $R_C \sim 24$  star-galaxy separation works well. In deeper surveys many sources have sizes comparable to the size of the PSF, and applying size cuts may change the redshift distribution of the sources in a systematic way. In addition, down to  $R_C \sim 24$  the redshift distribution of the sources is fairly well determined. In order to relate the observed cosmic shear signal to cosmological parameters, a good understanding of the source redshift distribution is crucial.

One worry is the effect of intrinsic alignments of the source galaxies, which introduces an additional signal (e.g., Heavens et al. 2000; Catelan et al 2001; Crittenden et al. 2001; Mackey et al. 2001). The amplitude of the effect is not well determined, but it is clear that it becomes more important for shallower surveys. However, the predictions indicate that for a median redshift of  $z = 0.5$  (which is similar to our sample of source galaxies) the signal caused by intrinsic alignments is still small compared to the lensing signal (e.g., Makey et al. 2001), and we will ignore the effect in this paper.

In §2 we describe the Red-Sequence Cluster Survey (RCS) from which we have used the  $R_C$ -band data for the analysis presented here. §3 deals with the analysis of the data, as well as the corrections for systematic distortions, such as PSF anisotropy and the distortion by the camera. In §4 we discuss the expected signal from weak lensing by large scale structure. The results of the analysis are presented in §5.

## 2. DATA

### 2.1. The Red-Sequence Cluster Survey

The Red-Sequence Cluster Survey<sup>1</sup> (RCS) is a galaxy cluster survey designed to provide a large sample of op-

tically selected clusters of galaxies with redshifts  $0.1 < z < 1.4$ . The planned survey will cover 100 square degrees in both  $R_C$  and  $z'$ , and consists of 22 widely separated patches of  $\sim 2.1 \times 2.3$  degrees. The northern half of the survey is observed using the CFH12k camera on the CFHT, and the data from the southern half are obtained using the Mosaic II camera on the CTIO 4m telescope. The patches are imaged down to a  $5\sigma$  point source depth of 25.2 magnitudes in the  $R_C$ -band, and 23.6 magnitudes in the  $z'$  filter.

For the weak lensing analysis we use only the  $R_C$  band data, as these provide a sufficiently high number density of sources to warrant an accurate measurement of the lensing signal. We present the results based on  $\sim 16.4$  deg<sup>2</sup> of CFHT data and  $\sim 7.6$  deg<sup>2</sup> of CTIO data. In this paper we use a subset of the RCS and the data for each patch are not contiguous. Thus the largest scale we consider here is that of one pointing of the CFH12k or Mosaic II camera.

We have used data from all 10 patches that have been observed using the CFHT, resulting in a total of 53 pointings. The integration times are 900s per pointing. In addition we have used three patches (resulting in an additional 23 pointings) from the first CTIO run, which have integration times of 1200s. Some details about the observations are listed in Table 1.

### 2.2. Data reduction

Given the large amount of data collected in the survey, special attention was paid during the survey design on how to handle the data flow. To simplify the construction of the science images the data were acquired without dithering. Although the gaps between the chips, cosmetic defects, and cosmic rays result in a minor loss in area, the advantage in handling the data flow is tremendous. The loss of area does not affect the result of the weak lensing analysis, and cosmic rays are easily removed from the galaxy catalogs.

The individual chips from the mosaic imagers are de-biased, and flat-fielded using standard techniques. The images are used for the object analysis, which is described below. A detailed discussion of the reduction pipeline is presented in Gladders & Yee (in preparation).

## 3. OBJECT ANALYSIS

Our weak lensing analysis technique is based on that developed by Kaiser, Squires & Broadhurst (1995) and Luppino & Kaiser (1997), with a number of modifications which are described in Hoekstra et al. (1998) and Hoekstra et al. (2000).

This correction scheme assumes that one can model the PSF as an isotropic function, convolved with a compact, anisotropic kernel. The method does not make any assumptions about the profile of the PSF or the galaxy, as these parameters are measured from the actual data.

In real data, the PSF is likely to be more complex, and the assumption stated above is not valid. However, as shown by Hoekstra et al. (1998) matching the measurement of the PSF parameters to the size of the galaxy results in accurate corrections for PSFs with varying ellipticity as a function of radius (as is the case for the WFPC2 PSF).

<sup>1</sup> <http://www.astro.utoronto.ca/~gladders/RCS>

patch	pointing	seeing ["]	run	pointing	seeing ["]	run
(a) CFHT						
0223	A2	0.72	2	B2	0.78	2
	A3	0.92	2	B3	0.79	2
	A4	0.77	2	B4	0.64	2
	A5	0.67	2	B5	0.64	2
0349	A1	0.69	2	C1	0.63	2
	A2	0.79	2	C2	0.59	2
	A3	0.87	2			
0920	A2	0.73	2	C2	0.60	1a
	B1	0.70	2	C3	0.69	1a
	B2	0.75	2			
1120	A3	0.80	2	B3	0.67	2
	A4	0.82	2	B4	0.69	2
	B2	0.76	2			
1326	A3	0.74	2	C2	0.55	1a
	A5	0.79	2	C3	0.58	1a
	C1	0.58	1a			
1417	B2	0.61	1a	B4	0.52	1a
	B3	0.61	1a	B5	0.59	1a
1447	A2	0.79	3	B2	0.66	2
	A3	0.74	3	B4	0.73	3
	B1	0.63	3			
1614	A1	0.59	1a	B2	0.56	1a
	A5	0.50	1a	B3	0.57	1a
	B1	0.56	1a			
2148	B2	0.63	1b	C1	0.89	1b
	B3	0.65	1b	C2	0.82	1b
	B4	0.69	1b			
2316	A1	0.69	3	B3	0.72	3
	A2	0.66	3	B5	0.74	3
	A3	0.66	3			
(b) CTIO						
0333	A3	0.97	1	B4	0.82	1
	A4	0.98	1	C3	1.03	1
	B3	0.88	1	C4	1.12	1
0438	A1	0.80	1	B3	0.89	1
	A2	0.84	1	B4	0.89	1
	A3	0.87	1	C3	0.94	1
1102	A4	0.94	1	C4	0.93	1
	A1	0.68	1	B4	0.77	1
	A2	0.75	1	C2	0.81	1
	A3	0.76	1	C3	0.86	1
	A4	0.82	1	C4	0.79	1
	B3	0.81	1			

TABLE 1

(a) Some information for the 53 CFHT pointings used in this analysis. Ten widely separated patches have been observed. Typically 5 pointings per patch were used, except for the 1417 (4 pointings) and the 0223 patch (8 pointings); (b) Information for the 23 CTIO pointings. We used all the data obtained during run 1, and as a result the number of pointings per patch varies. The seeing was determined for both telescopes using the sizes of stars on chip 3.

In addition, the accuracy of this method has been studied in great detail (e.g., Erben et al. 2001; Bacon et al. 2001) and the results demonstrate that it works well down to the required accuracy for current data sets. Hence, the correction scheme is accurate even if the PSF does not satisfy the assumption made in the derivation. However, this can be understood easily, because any residuals induced by higher order moments of the PSF are suppressed as one averages the shapes of galaxies which have random

orientations with respect to the PSF.

We analyse the chips of each pointing separately. After the catalogs have been corrected for the various observational effects, they are combined into a master catalog which covers the observed field (for each pointing).

The first step in the analysis is to detect the faint galaxy images, for which we used the hierarchical peak finding algorithm from Kaiser et al. (1995). We select objects which are detected with a significance greater than  $5\sigma$  over the local sky.

We use single exposures for our analysis, and consequently cosmic rays have not been removed. However, cosmic rays are readily eliminated from the photometric catalogs: small, but very significant objects are likely to be cosmic rays, or artefacts from the CCD. The peak finder gives fair estimates of the object size, and we remove all objects smaller than the size of the PSF.

The objects in this cleaned catalog are then analysed, which yield estimates for the size, apparent magnitude, and shape parameters (polarization and polarizabilities). The objects in this catalog are inspected by eye, in order to remove spurious detections. These objects have to be removed because their shape measurements are affected by cosmetic defects (such as dead columns, bleeding stars, halos, diffraction spikes) or because the objects are likely to be part of a resolved galaxy (e.g., HII regions). The visual inspection is important as it is not possible to remove all spurious detections in a fully automatic process. Their removal is crucial for an accurate measurement of cosmic shear, because they increase the measurement of the variance, and introduce artificial ellipticity correlations.

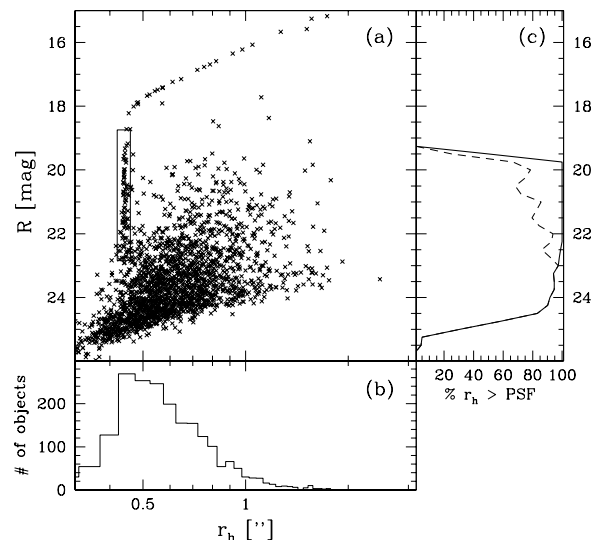


FIG. 1.— (a) Plot of the apparent  $R_C$ -band magnitude versus the half-light radius. The vertical sequence of points at  $r_h \sim 0''.45$  (indicated by the rectangle) consists of bright, unsaturated stars, that are used to study the PSF. (b) Histogram of the number of objects of given  $r_h$ . (c) The dashed line shows the fraction of objects with half light radii larger than the PSF. The solid line shows the fraction of objects larger than the PSF, when the total counts are corrected for the contribution by stars. Objects larger than the PSF are assumed to be galaxies and only these are used in the weak lensing analysis. The figure demonstrates that down to  $R \sim 24$  this separation selects most galaxies, as almost all objects are larger than the PSF.

### 3.1. Correction for the PSF

To measure the small, lensing induced distortions in the images of the faint galaxies it is important to accurately correct the shapes for observational effects, such as PSF anisotropy and seeing; PSF anisotropy can mimic a cosmic shear signal, and a correction for the seeing is required to relate the measured shapes to the real lensing signal.

To do so, we follow the procedure outlined in Hoekstra et al. (1998). We select a sample of moderately bright stars from our observations, and use these to characterize the PSF anisotropy and seeing. Figure 1a shows a plot of the apparent  $R_C$ -band magnitudes of the detected objects versus their measured half-light radii for one of the chips of the A2 pointing of the 0223 patch (seeing  $\sim 0''.77$ ). We have also indicated the region from which we have taken the stars used for the analysis of the PSF.

We fit a second order polynomial to the shape parameters of the selected stars for each chip. This procedure is repeated for various dispersions of the weight function (for details see Hoekstra et al. 1998). In the left panel of Figure 2 we present the resulting model PSF anisotropy for the A2 pointing of the 0223 patch. To show in more detail the higher order spatial dependence of the anisotropy we have subtracted the average ellipticity. Although the fits were obtained from the individual chips, the mosaic image in Figure 2 shows continuity between the chips.

The results for one of the CTIO pointings is presented in the right panel of Figure 2. Comparison of the patterns presented in Figure 2 with other pointings shows that the pattern is fairly stable, although the amplitude varies, because of focus variations. In general the PSF anisotropy is small, a point which we will address in more detail below,

when we examine the residuals left after correction of the shapes of the galaxies used in the weak lensing analysis.

### 3.2. Telescope distortion

The effect of the PSF is not the only observational distortion that has to be corrected. The optics of the camera stretches the images of galaxies (i.e., it introduces a shear) because of the non-linear remapping of the sky onto the CCD. We have used observations of astrometric fields to find the mapping between the sky and the CCD pixel coordinate system, and derived the corresponding camera shear.

The camera shear for the CFH12k camera for run 2 is presented in Figure 3. The shear introduced by the camera is small, reaching a maximum value of  $\sim 1\%$  at the edges of the field of view.

Other weak lensing studies, which use dithered observations, need to remap the images before combining the data, thus removing the camera distortion. We have analysed single exposures, and measured the shapes of the galaxies on the reduced images that have not been remapped to remove the camera distortion. As discussed in Hoekstra et al. (1998), the images of both the stars and galaxies are sheared by the camera. The measured shape of the PSF (as shown in Figure 2) is then the combination of PSF anisotropy and camera shear, and therefore the real PSF anisotropy is somewhat smaller than the measured value. The change in the ellipticity of an object caused by the camera shear depends on its shape (and hence the correction) whereas the PSF anisotropy correction depends mainly on the size of the object. As a result the correction for PSF anisotropy leaves a residual ellipticity, because the correction will be too large for larger galaxies. However,

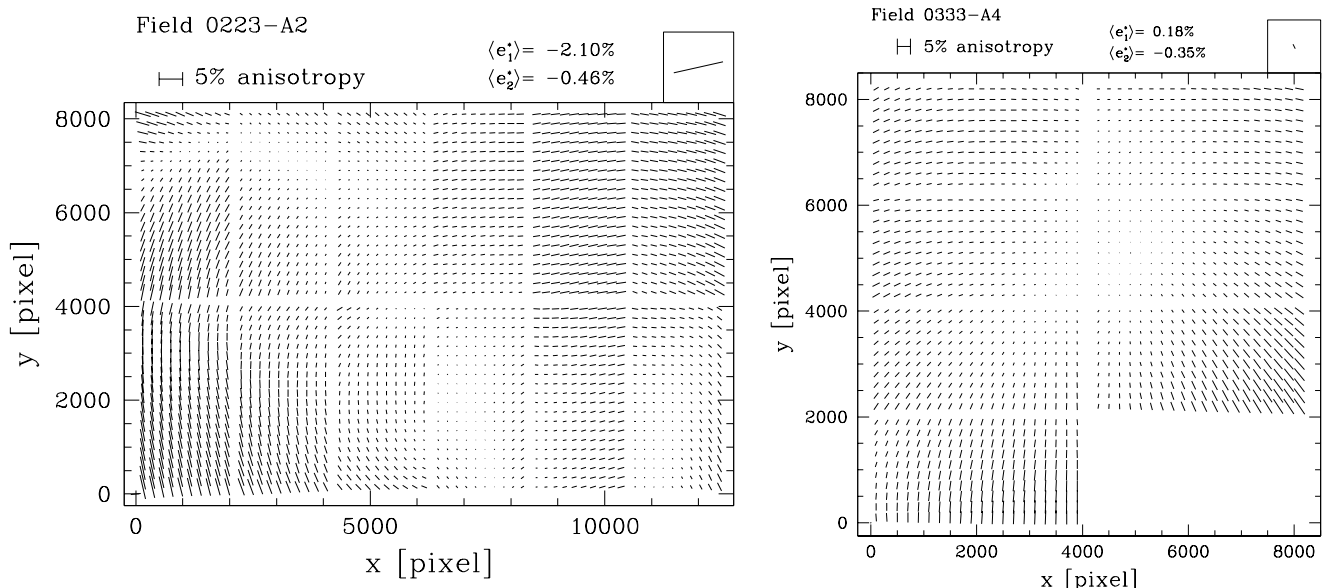


FIG. 2.— Left panel: PSF anisotropy as a function of position for one of the CFHT pointings; right panel: PSF anisotropy for one of the CTIO pointings. One of the chips in the CTIO observations was not functioning and has been omitted. The sticks indicate the direction of the major axis of the PSF, and the length is proportional to the observed ellipticity of the PSF. In order to show the higher order spatial dependence of the anisotropy we have subtracted the average ellipticity. The direction of the average PSF anisotropy is indicated in the top right box, and the amplitude is indicated as well. Although the PSF anisotropy was determined from fits to the observed shapes for individual chips, the figure clearly shows a large scale dependence.

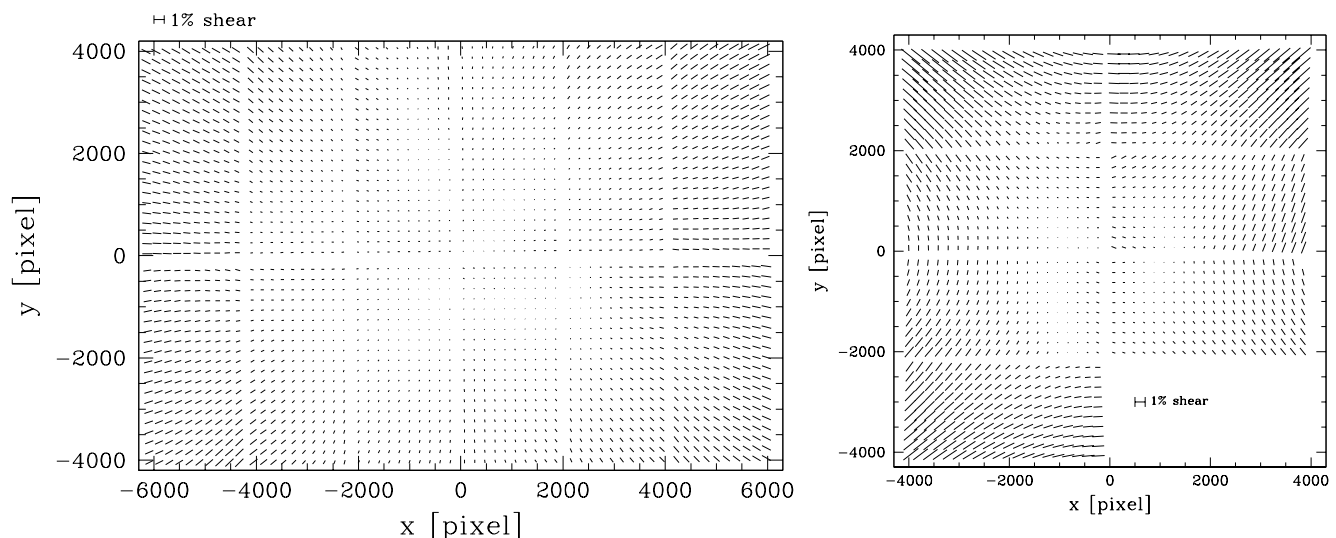


FIG. 3.— Left panel: camera distortion measured for the CFH12k camera for run 2. The shear introduced by the camera is small, reaching a maximum value of  $\sim 1\%$  at the edges of the field of view; Right panel: the camera distortion measured from the CTIO data. One of the chips was not functioning and has been omitted. The induced shear by this camera is somewhat larger than the CFH12k camera, but still small:  $\sim 2\%$  at the edges of the field of view.

Hoekstra et al. (1998) demonstrated that the correction for the residual camera shear is straightforward: one just needs to subtract the camera shear from the measured shear, which is what we have done.

The camera shear is more or less radial with respect to the center of the camera (although the camera shear of the CTIO Mosaic II camera shows a significant non-radial component), which results in a negative tangential shear. It is therefore useful to examine the average tangential shear of the galaxies with respect to the center of the camera. The results are presented in Figure 4a. The solid circles indicate the average tangential distortion of the galaxies with respect to the center of the CFH12k camera after correction for PSF anisotropy. These measurements agree well with inferred camera shear (solid line). After subtracting the camera shear we obtain the open circles, which are consistent with no signal.

### 3.3. Residuals

The correction scheme developed by Kaiser et al. (1995) has been tested extensively (e.g., Hoekstra et al. 1998; Bacon et al. 2001; Erben et al. 2001). The assumptions that have to be made to derive the original Kaiser et al. (1995) correction parameters do not necessarily hold in real data, the modifications suggested by Hoekstra et al. (1998) allow it to be applied to more complicated PSFs. This is supported by numerous simulations which indicate the method works remarkably well down to the required accuracy for current data sets.

In addition we have tested the method using a realistic simulation. The simulated data sets were created using the software tools *SkyMaker* and *Stuff*<sup>2</sup>, which have been described in detail in Erben et al. (2000). The simulated galaxies have realistic profiles, with a mix of early type, late type galaxies, and disk/bulge ratios matched to actual observations. The PSF is computed using realistic pupil

functions, and includes all the problems encountered in real data, such as coma, tracking errors, aberration, spider arms from the support of the secondary mirror, etc.

The simulation is described by Van Waerbeke et al. (in preparation), and here we briefly discuss the results. Van Waerbeke used an N-body simulation to infer the corresponding (cosmic) shear by means of ray-tracing.

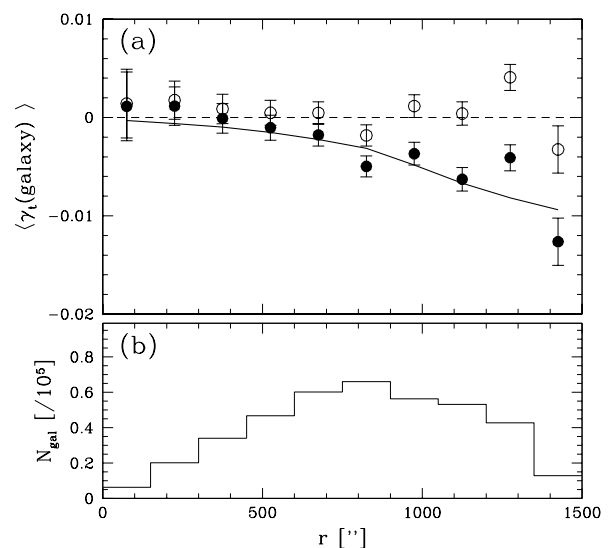


FIG. 4.— (a) Solid circles indicate the average tangential distortion of the galaxies with respect to the center of the CFH12k camera after correction for PSF anisotropy. The solid line corresponds to the average tangential camera shear. The open circles give the measurements of the galaxies after correcting for both PSF anisotropy and camera distortion. The results indicate that the two steps in the correction have worked well. (b) number of galaxies as a function of radius used to produce panel (a).

<sup>2</sup> see <http://terapix.iap.fr/soft>

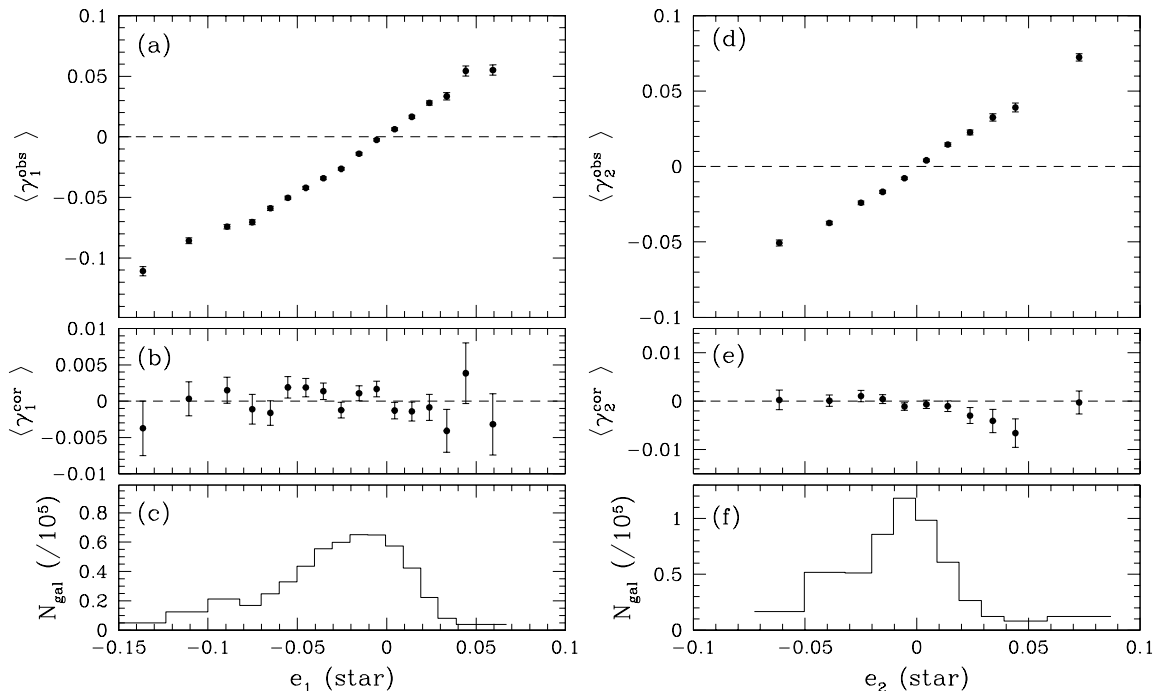


FIG. 5.— (a)  $\langle \gamma_1 \rangle$  for the galaxies with  $20 < R < 24$  as a function of the value of the ellipticity component  $e_1$  of the stars used to correct the galaxies. The results show the expected strong correlation; (b) The average  $\gamma_1$  after correction for PSF anisotropy (note the vertical scale has been expanded with respect to panel a); (c) The number of galaxies with a given value for  $e_1$  of the PSF; (d)-(f) same as (a)-(c), but for  $\gamma_2$ . The residuals are consistent with no signal, demonstrating that the correction for the PSF anisotropy has worked well.

Artificial images of galaxies were sheared using these results. These galaxies were “observed” and the final images are convolved with a realistic PSF. A mosaic of 900 images (corresponding to  $\sim 12 \text{ deg}^2$ ), each with a different PSF was given to us. We note that the PSFs used in the simulation had worse systematics than the once observed in the RCS data.

We analysed these images in the same way as we have analysed the RCS data, and measured the cosmic shear signal. In doing so, we were able to recover the input lensing signal, which was unknown to us. We were able to recover the signal within 10% ( $\sim 1\sigma$ ) of the input value. Because of the noise introduced by the intrinsic shapes of the galaxies, larger simulations are required to test whether we can measure the lensing signal to even higher accuracies.

We have also examined the residuals in the RCS data after PSF correction. A useful test, although not definitive, is to plot the average shape of the galaxies as a function of the shape of the PSF. The results for the two components of the shear are presented in Figure 5. Panels (c), and (f) indicate that the PSF anisotropy is small for most galaxies. The residuals presented in panels (b), and (e) (note the different vertical scale) are consistent with no signal. The results of Figure 5 and the results from the simulation suggest that we are able to measure the lensing signal to an accuracy better than 10%.

#### 4. COSMIC SHEAR SIGNAL

To study the weak lensing signal caused by large scale structure, we use the top-hat smoothed variance of the shear (Bacon et al. 2000; Kaiser et al. 2000; Maoli et

al. 2001; van Waerbeke et al. 2000; van Waerbeke et al. 2001). Other statistics, such as the ellipticity correlation function (Kaiser 1992; van Waerbeke 2001; Wittman et al. 2000) or the aperture mass statistic (Schneider 1998, Schneider et al. 1998; van Waerbeke 2001) have also been used.

Here we briefly discuss how the lensing signal depends on the assumed cosmology and the redshift distribution of the sources. Detailed discussions on this subject can be found elsewhere (e.g., Schneider et al. 1998; Bartelmann & Schneider 2001).

Given a cosmological model, the variance in the shear caused by large scale structure can be computed as a function of aperture size  $\theta$  (e.g., Jain & Seljak 1997):

$$\langle \gamma^2 \rangle(\theta) = 2\pi \int_0^\infty dl l P_\kappa(l) \left[ \frac{J_1(l\theta)}{\pi l \theta} \right]^2, \quad (1)$$

where  $\theta$  is the radius of the aperture used to compute the variance, and  $J_1$  is the first Bessel function of the first kind. The effective convergence power spectrum  $P_\kappa(l)$  is given by

$$P_\kappa(l) = \frac{9H_0^4 \Omega_m^2}{4c^4} \int_0^{w_H} dw \left( \frac{\bar{W}(w)}{a(w)} \right)^2 P_\delta \left( \frac{l}{f_K(w)}; w \right). \quad (2)$$

Here  $w$  is the radial coordinate,  $w_H$  corresponds to the horizon,  $a(w)$  the cosmic scale factor, and  $f_K(w)$  the comoving angular diameter distance. As shown by Jain & Seljak (1997) and Schneider et al. (1998) it is necessary to use the non-linear power spectrum in equation (2). This

power spectrum is derived from the linear power spectrum following the prescriptions from Peacock & Dodds (1996).

$\bar{W}(w)$  is the source-averaged ratio of angular diameter distances  $D_{ls}/D_s$  for a redshift distribution of sources  $p_w(w)$ :

$$\bar{W}(w) = \int_w^{w_H} dw' p_w(w') \frac{f_K(w' - w)}{f_K(w')}. \quad (3)$$

Thus it is important to know the redshift distribution of the sources, in order to relate the observed signal to  $P_\kappa(l)$ . A detailed discussion of the adopted redshift distribution can be found in Section 4.1. Figure 6 shows the top-hat smoothed variance  $\langle \gamma^2 \rangle$  on a scale of 1 arcminute as a function of limiting magnitude of the sample of sources. To compute the signal we used galaxies with  $20 < R < R_{\text{lim}}$  and used the photometric redshift distribution inferred from the Hubble Deep Fields north and south (see section 4.1). The top axis indicates the corresponding median redshift of the source galaxies.

One of the advantages of deep observations is obvious from Figure 6: the signal increases quickly for limiting magnitudes fainter than  $R = 24$  (or higher median redshift). In addition the number of sources increases as well, resulting in higher signal-to-noise ratios of the measurements.

#### 4.1. Redshift distribution

In order to relate the observed lensing signal to physical parameters, such as  $\sigma_8$  or  $\Omega_m$ , knowledge of the redshift distribution of the sources is crucial. The galaxies used in weak lensing surveys are generally too faint to be included in redshift surveys, and little is known about their redshift distribution from spectroscopic studies.

Compared to the other, deeper, cosmic shear studies, our analysis has the major advantage that the redshift distribution of the sources we use is better known. Down to a limiting magnitude of  $R_C = 24$  the redshift distribution has been determined spectroscopically by Cohen et al. (2000), although this survey is limited to a relatively small patch of sky, and is likely to suffer from cosmic variance.

In addition the galaxies are larger, which is demonstrated in Figure 1: down to  $R_C = 24$  the galaxies are easily separated from the stars. This has the advantage over deeper surveys (where the fainter galaxies have sizes comparable to the PSF) in that selecting objects larger than the PSF does not change the redshift distribution significantly. Even for the worst seeing images considered here ( $\sim 1''.1$ ) the stars are well separated from the galaxies for  $R_C = 24$ .

Photometric redshift studies, in particular those based on the Hubble Deep Fields (e.g., Fernández-Soto et al. 1999; Chen et al. 1998) have also provided important information. The results of Hoekstra et al. (2000) have demonstrated that they generally work well. However, Hoekstra et al. (2000) noted a difference between the redshift distributions inferred for the Northern and the Southern field, and such field to field variation is not unexpected. However, currently little is known about the amplitude of such variations, and more studies are required to constrain the redshift distributions of these faint galaxies.

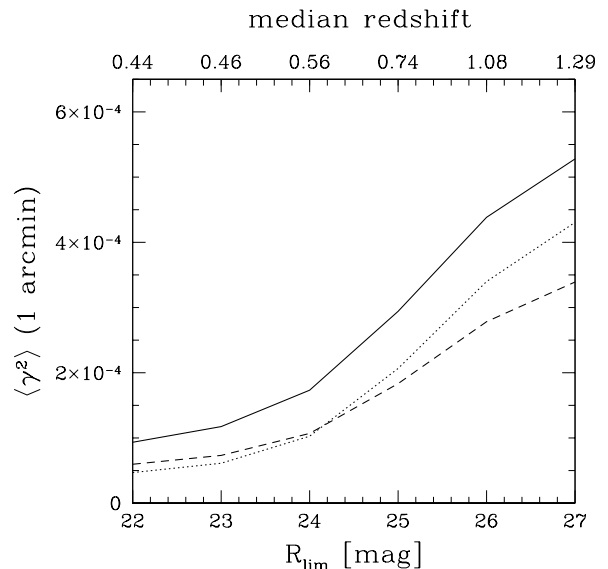


FIG. 6.— The expected variance induced by large scale structure in an aperture of radius 1 arcminute, as a function of limiting magnitude of the source galaxies. To derive these results we used source galaxies fainter than  $R = 20$ , and assumed perfect shape measurements. The result for the SCDM (solid line,  $\Omega_m = 1$ ,  $\Omega_\Lambda = 0$ ,  $\sigma_8 = 0.5$ ,  $\Gamma = 0.5$ ), OCDM (dashed line,  $\Omega_m = 0.3$ ,  $\Omega_\Lambda = 0$ ,  $\sigma_8 = 0.85$ ,  $\Gamma = 0.21$ ) and LCDM (dotted line,  $\Omega_m = 0.3$ ,  $\Omega_\Lambda = 0.7$ ,  $\sigma_8 = 0.9$ ,  $\Gamma = 0.21$ ) are shown. The cosmic shear signal increases rapidly with increasing limiting magnitude, or increasing median redshift (as indicated by the top axis).

In order to minimize the contribution of cosmic variance to the redshift distribution, we use the photometric redshift distributions from Fernández-Soto et al. (1999) and Chen et al. (1998) to compute the predicted lensing signal for a given cosmology (see Fig. 2 from Hoekstra 2001 for the resulting redshift distribution). To do so, we have to take into account that the uncertainty in the shape measurements depend on the apparent magnitudes (and thus on the redshifts) of the sources: the contribution of distant, small faint galaxies (with noisy shape measurements) to the measured lensing signal is smaller compared to brighter galaxies.

This is illustrated in Figure 7. Figure 7a shows the expected (based on modeling of deep number counts), the observed (galaxies for which shapes could be measured), and effective number counts (dotted line) as a function of apparent magnitude. The effective number density takes into account the uncertainty in the galaxy shapes, and gives a good indication of which galaxies contribute most to the measurement of the lensing signal. Based on the results displayed in Figure 7, we decided to use galaxies with  $20 < R_C < 24$  for the lensing analysis.

The relative weight (normalised to unity for bright galaxies) as a function of magnitude is shown in Figure 7b. This weight function is simply the inverse square of the uncertainty in the shape measurement (see Hoekstra et al. 2000 for details), and reflects the fact that the shapes estimates of faint galaxies are more noisy. We derive the “effective” redshift distribution using this weight function. This effective redshift distribution is used to compute the predicted lensing signals discussed in Section 5.

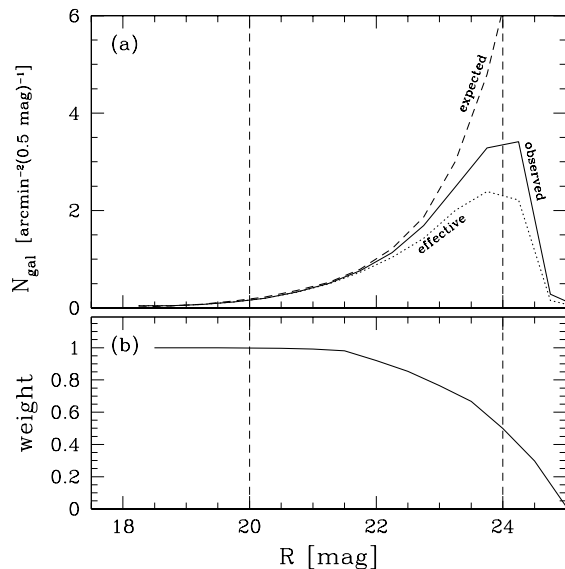


FIG. 7.— (a) Observed number density of galaxies (i.e. galaxies for which shapes could be determined) as a function of apparent  $R_C$  magnitude (solid line). The expected number density (based on modeling of observed number counts) is indicated by the dashed line. (b) The weight (based on the uncertainty in the shape measurements; see Hoekstra et al. 2000) multiplied by the completeness fraction as a function of apparent magnitude. The product of the number of galaxies and the weight gives a good indication of the relative contribution to the lensing signal (dashed line in panel (a)). The result shows that most of the signal comes from galaxies around  $R_C = 23.5$ . The vertical dashed lines indicate the region  $20 < R_C < 24$ , the range of apparent magnitudes for the source galaxies we will use in the lensing analysis.

## 5. RESULTS

### 5.1. Observed signal

In this section we present the measurement of the weak lensing signal caused by large scale structure using the top-hat smoothed variance of the shear. This statistic has been used by other groups to detect the cosmic shear signal (e.g., Bacon et al. 2000; Kaiser et al. 2000; Maoli et al. 2001; Van Waerbeke et al. 2000, 2001). The top-hat smoothed variance is fairly insensitive to errors in the analysis because residual shears are added in quadrature. Consequently the observed signal can always be considered as an upper limit, because residual errors always increase the variance. However, the results presented in Figure 5 and the simulations discussed in section 3.3 indicate that we can measure the shapes of the galaxies accurately.

As was found by van Waerbeke et al. (2000), close pairs of galaxies can introduce an excess signal, because of overlapping isophotes. We therefore remove pairs with a separation of less than  $2''.16$  (which corresponds to 10 pixels for the CFHT data, and 8 pixels for the CTIO data). This lowered the signal at small scales ( $\sim 20\%$  for an aperture of radius 1 arcminute). We note that on these scales intrinsic alignments can also be important. To compute the top-hat smoothed variance we use the practical estimators given in Van Waerbeke et al. (2001).

Figure 8 shows the top-hat smoothed variance as a function of scale for both the CFHT data (filled circles) and the CTIO data (open circles) using galaxies with  $20 < R_C < 24$ . The errorbars are estimated from a large

number of random realisations of the data set where the orientations of the galaxies were randomized.

Note that the measurements at various scales are strongly correlated, and this causes all the CTIO measurements at large scales to be higher than the CFHT results. The results obtained from the two different telescopes agree very well with one another. Because the systematics for the two data sets are different, this excellent agreement demonstrates that the various observational biases have been removed successfully.

Another useful test is to compare the signals from the individual patches. Figure 9 displays the top-hat smoothed variance of the shear for an aperture of radius 2.5 arcminutes (where the signal-to-noise ratio is highest) for the 13 observed patches. The measurements for the individual patches agree with the ensemble average.

It is also important to examine the correction for the circularization by the PSF, because it determines the amplitude of the signal. To do so, we computed the variance on a scale of 2.5 arcminutes for each pointing, and looked for a correlation with seeing. The results show no trend with seeing.

Figure 10 shows the measurement of the top-hat smoothed variance for the full weak lensing data set. The signal-to-noise ratio of our measurements is very good, reaching a maximum of  $\sim 6$  at a radius of 2.5 arcminutes.

For comparison the predictions for three different cosmological models are also shown in this figure. All three models are good fits to the data, indicating the need for additional observational constraints (cf. §5.2)

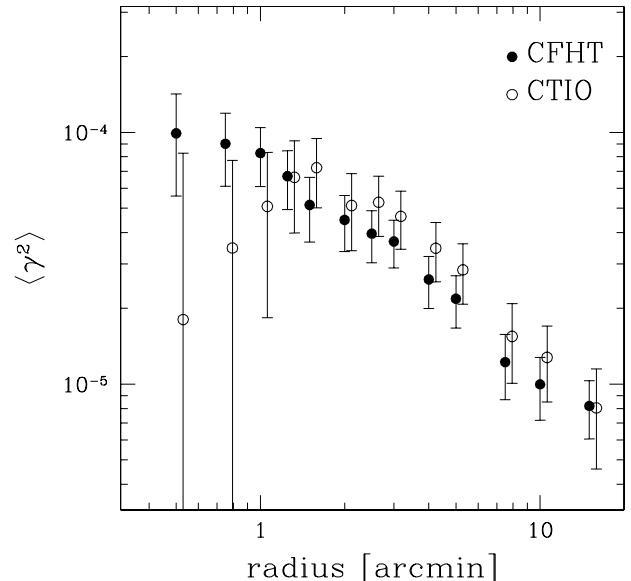


FIG. 8.— Top-hat smoothed variance of the shear as a function of aperture radius. The filled circles indicate the measurements based on  $16.4 \text{ deg}^2$  of CFHT data, and the open circles correspond to the analysis of  $7.6 \text{ deg}^2$  of CTIO data. For display purposes the CTIO points have been offset slightly in radius. Note that the measurements at various scales are strongly correlated, and this causes all the CTIO measurements at large scale to be higher than the CFHT results. The results obtained from the two different telescopes agree well with one another.



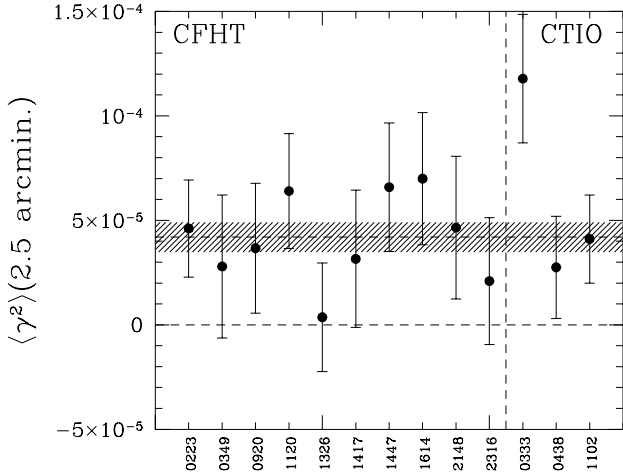


FIG. 9.— The top-hat smoothed variance of the shear for an aperture of radius 2.5 arcminutes for the 13 observed patches. The shaded region corresponds to the  $1\sigma$  limits around the average. The measurements for the individual patches agree well with the average, indicating that the cosmic variance is small.

It is difficult to compare our measurements directly to most other studies, because of the difference in the source redshift distribution (caused by the difference in filters and integration times). However, we can compare directly to the results from Bacon et al. (2000), who have used a similar cut in apparent magnitude. Bacon et al. (2000) find a variance of  $\langle \gamma^2 \rangle = (24 \pm 7) \times 10^{-5}$  in  $8 \times 8$  arcminute cells. This scale is similar to a radius of  $\sim 4$  arcminutes for which we find  $\langle \gamma^2 \rangle = (2.8 \pm 0.5) \times 10^{-5}$ . Our signal is much lower than their result. Bacon et al. (2000) note a residual correlation between the shape of the PSF and the galaxies (their Fig. 7), and this might explain their increased variance. We note that because of the large errorbar on the measurement of Bacon et al. (2000) the results are consistent at the  $3\sigma$  level.

### 5.2. Constraints on cosmological parameters

As described in Section 4 the predicted amplitude of the top-hat smoothed variance depends on the various cosmological parameters, and therefore provides a powerful method to constrain these parameters. Unfortunately several degeneracies exist (e.g., Bernardeau et al. 1997; Jain & Seljak 1997). These studies show that the amplitude of the signal is mainly determined by a combination of  $\sigma_8$  and  $\Omega_m$ , although the shape parameter  $\Gamma$  ( $\sim \Omega_m h$  in a CDM cosmology) is also important.

As demonstrated by Van Waerbeke et al. (2001), it is possible to partially break the degeneracy between  $\sigma_8$  and  $\Omega_m$  if priors on the shape of the power spectrum are assumed. The value of  $\Omega_\Lambda$  can be constrained by combining the measurements of the lensing signal for sources at different redshifts, using the fact that the angular diameter distances depend on  $\Omega_\Lambda$ . The combination of the weak lensing measurements and the constraints from studies of the fluctuations of the cosmic microwave background (CMB) will provide much stronger constraints of the parameters, as the combination will break the degeneracies.

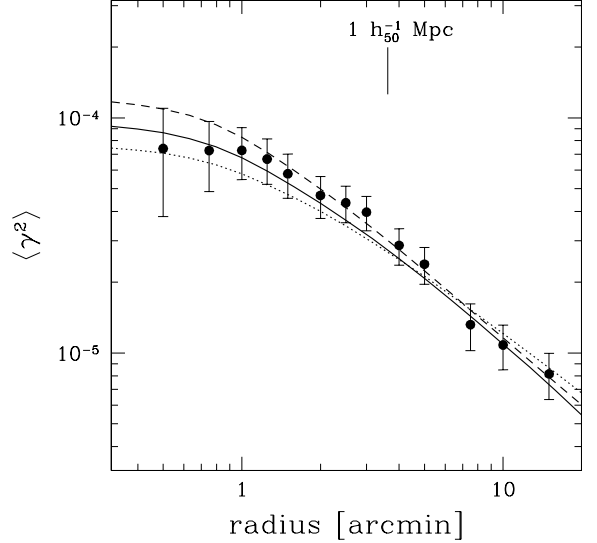


FIG. 10.— Measurement of the top-hat smoothed variance (excess variance caused by lensing by large scale structure) using galaxies with  $20 < R_C < 24$ . The data consist of  $16.4 \text{ deg}^2$  of CFHT data and  $7.6 \text{ deg}^2$  of CTIO data. The drawn lines correspond to the best fit SCDM ( $\Omega_m = 1$ ,  $\Omega_\Lambda = 0$ ,  $\Gamma = 0.7$ ,  $\sigma_8 = 0.31$ ; solid line), the best fit OCDM ( $\Omega_m = 0.3$ ,  $\Omega_\Lambda = 0.0$ ,  $\Gamma = 0.21$ ,  $\sigma_8 = 0.86$ ; dashed line), and the best fit  $\Lambda$ CDM ( $\Omega_m = 0.3$ ,  $\Omega_\Lambda = 0.7$ ,  $\Gamma = 0.21$ ,  $\sigma_8 = 0.81$ ; dotted line) model. We fixed  $h = 0.7$ , which gives a high value for  $\Gamma$  for the SCDM model. Without additional constraints on the cosmological parameters, the lensing results are consistent with a wide range of cosmological models. The errorbars are estimated from a large number of random realisations of the data set where the orientations of the galaxies were randomized. Note that the points at various scales are strongly correlated. Under the assumption that the lensing structures are halfway between the observer and the sources, we have indicated a scale of  $1 h_{50}^{-1} \text{ Mpc}$ .

Here we will use the measurements of the top-hat smoothed variance to find constraints on  $\Omega_m$  and  $\sigma_8$ . We assume that the measurements follow a normal distribution. We computed the covariance matrix from a large number of random realisations of the data, thus including the survey geometry in the noise correlation.

We compute the model predictions using equation 3, under the assumption that  $\Gamma = 0.21$ , and using the effective redshift distribution discussed in section 4.1. We use this value for  $\Gamma$  to allow for a direct comparison with the results from Van Waerbeke et al. (2001). The predictions are compared to the observations, and the likelihood for the combination of  $\Omega_m$  and  $\sigma_8$  is computed. The results for models with  $\Omega_\Lambda = 0$  are presented in Figure 11. The contours indicate the 68.3%, 95.4%, and 99.7% confidence limits on two parameters jointly.

The results for the  $\Omega_m + \Omega_\Lambda = 1$  model are presented in Figure 12. The best fit value for  $\Omega_m$  is lower than for the OCDM model, but no strong constraints on  $\Omega_m$  and  $\sigma_8$  can be placed. Allowing for larger values ( $\Gamma \sim 0.7$ ), the goodness of fit for high  $\Omega_m$  models is comparable to those of low  $\Omega_m$  models. We note, however, that studies of the galaxy correlation function suggest values for  $\Gamma = 0.1 - 0.3$  (e.g., Dodelson et al. 2001).

The best fit  $\Lambda$ CDM cosmology yields  $\sigma_8 = 0.81^{+0.14}_{-0.19}$  (95% confidence;  $\Gamma = 0.21$ ). For the best fit OCDM model we obtain  $\sigma_8 = 0.86^{+0.14}_{-0.17}$  (95% confidence). Van Waerbeke

et al. (2001) find  $\sigma_8 = 0.99^{+0.08}_{-0.10}$  (95% confidence) for an  $\Lambda$ CDM model, which is in fair agreement with our result, in particular when the uncertainty in the redshift distribution used by Van Waerbeke et al. (2001) is taken into account.

To investigate the agreement between the CFHT and CTIO data we also computed the best fit values for  $\sigma_8$  for the two data sets. We obtain  $\sigma_8 = 0.84 \pm 0.09$  (68% confidence) for the CFHT data, and  $\sigma_8 = 0.76 \pm 0.12$  (68% confidence) for the CTIO data. The values agree well, and the probability of finding a smaller difference is 40%.

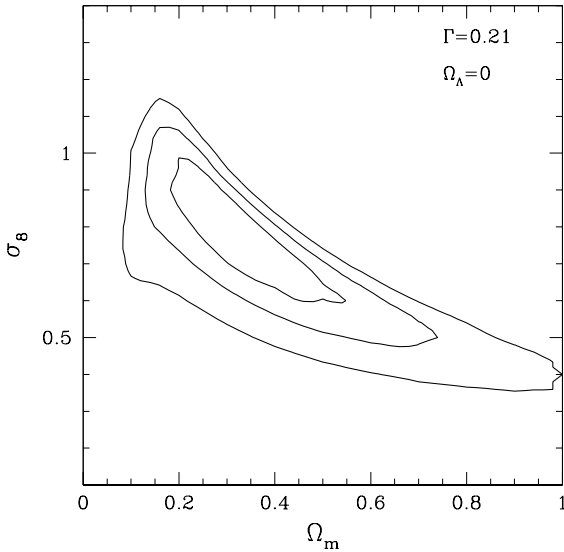


FIG. 11.— Likelihood contours as a function of  $\Omega_m$  and  $\sigma_8$ , inferred from the analysis of the top-hat smoothed variance. We have used only the measurements at radii  $\geq 1$  arcminute. The contours have been computed by comparing the measurements to CDM models with  $n = 1$ ,  $\Gamma = 0.21$  and  $\Omega_\Lambda = 0$ . The contours indicate the 68.3%, 95.4%, and 99.7% confidence limits on two parameters jointly.

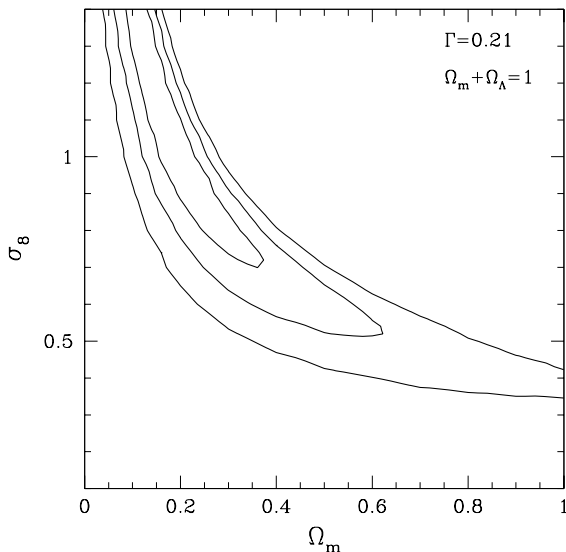


FIG. 12.— Same as Figure 11, but now for an  $\Omega_m + \Omega_\Lambda = 1$  CDM cosmology.

The RCS probes a different redshift range than the study presented by Van Waerbeke et al. (2001). Although both results are based on the same correction scheme, there are many differences in the various steps in the analyses. Thus the agreement found here suggests that accurate measurements of cosmic shear can be made.

## 6. CONCLUSIONS

We have analysed  $\sim 24$  square degrees of  $R_C$ -band imaging data from the Red-Sequence Cluster Survey to study the weak lensing signal caused by intervening large scale structure. To minimize the effect of cosmic variance, the measurements have been obtained from 13 patches that are widely separated on the sky. We have used data from two different telescopes:  $\sim 16.4$  square degrees of CFHT data and  $\sim 7.6$  square degrees of CTIO data. We detect the signal with high confidence on scales ranging from 1 to 30 arcminutes using galaxies with  $20 < R_C < 24$ .

Because of the various observational distortions which need to be corrected for, a careful analysis of the residuals is important. The results suggest that we have successfully corrected for the systematics. In addition we compared the measurements from CFHT and CTIO and find excellent agreement.

Compared to other studies of cosmic shear, the RCS imaging data is relatively shallow. This has the disadvantage that the lensing signal is low. However, the galaxies are larger (which results in smaller corrections for the PSF), and the redshift distribution is known fairly well (which is important for determining cosmological parameters).

Intrinsic alignments of galaxies contaminate the lensing signal. This is particularly important for lensing studies that use low redshift galaxies. The median redshift of our sample of sources is  $\sim 0.5$ , and predictions of the contribution of the intrinsic alignments suggest it is small for the results presented here. However, the effect of intrinsic alignments is expected to be comparable to the errorbars of the full RCS data set, and eventually needs to be corrected for. The RCS will be complemented with  $B$  and  $V$  band imaging which will provide photometric redshifts for a large number of galaxies. With such a data set we will be able to measure the intrinsic alignments by selecting galaxies at similar photometric redshifts.

We use the photometric redshift distribution inferred from the Hubble Deep Fields to relate the measured top-hat smoothed variance to estimates of cosmological parameters. Because of degeneracies in the parameters we can only place constraints on  $\Omega_m$  and  $\sigma_8$  jointly. For the currently favoured  $\Lambda$ CDM model ( $\Omega_m = 0.3$ ,  $\Omega_\Lambda = 0.7$ ,  $\Gamma = 0.21$ ) we obtain  $\sigma_8 = 0.81^{+0.14}_{-0.19}$  (95% confidence), in good agreement with the results from Van Waerbeke et al. (2001).

The RCS data and the observations used by Van Waerbeke are quite different, and also the weak lensing analyses are somewhat different. Thus the agreement found here suggests that accurate measurements of cosmic shear can be made.

It is a pleasure to thank Ludo van Waerbeke for many discussions, and providing a useful test of the correction scheme used in this paper. We would like to thank the

CFHT and CTIO TACs for their generous allocation of telescope time. This research is partially supported via an operating grant from NSERC to HKCY. MDG acknowledges support from NSERC via PGSA and PGSB scholar-

ships. PBH acknowledges financial support from Chilean grant FONDECYT/1010981. LFB's research is funded by FONDECYT, Chile under Proyecto 1000537.

## REFERENCES

- Bacon, D., Refregier, A., & Ellis, R.S. 2000, *MNRAS*, 325, 1065  
 Bacon, D., Refregier, A., Clowe, D., & Ellis, R.S. 2001, *MNRAS*, 325, 1065  
 Bartelmann, M., & Schneider, P. 2001, *Physics Reports*, 340, 291  
 Bernardeau, F., van Waerbeke, L., Mellier, Y. 1997, *A&A*, 322, 1  
 Blandford, R.D., Saust, A.B., Brainerd, T.G., & Villumsen, J.V. 1991, *MNRAS*, 251, 600  
 Catelan, P., Kamionkowski, M., & Blandford, R.D. 2001, *MNRAS*, 320, L7  
 Chen, H.-W., Fernández-Soto, A., Lanzetta, K.M., Pascarelle, S.M., Puetter, R.C., Yahata, N., & Yahil, A., preprint, astro-ph/9812339  
 Cohen, J.G., Hogg, D.W., Blandford, R.G., Cowie, L.L., Hu, E., Songaila, A., Shopbell, P., & Richberg, K. 2000, *ApJ*, 538, 29  
 Crittenden, R.G., Natarajan, P., Pen, U.-L., & Theuns, T. 2001, *ApJ*, submitted, astro-ph/0009052  
 Dodelson, S. et al. 2001, *ApJ*, preprint, astro-ph/0107421  
 Erben, T., Van Waerbeken, L., Bertin, E., Mellier, Y., & Schneider, P. 2001, *A&A*, 368, 766  
 Fernández-Soto, A., Lanzetta, K.M., & Yahil, A. 1999, *ApJ*, 513, 34  
 Gladders, M.D., & Yee, H.K.C. 2000, to appear in "The New Era of Wide-Field Astronomy", astro-ph/0011073  
 Gladders, M.D., Yee, H.K.C., & Ellingson, E. 2001, *AJ*, accepted  
 Heavens, A., Refregier, A., & Heymans, C. 2000, *MNRAS*, 319, 649  
 Hoekstra, H., Franx, M., Kuijken, K., & Squires, G. 1998, *ApJ*, 504, 636  
 Hoekstra, H., Franx, M., Kuijken, K. 2000, *ApJ*, 532, 88  
 Hoekstra, H., Franx, M., Kuijken, K., Carlberg, R.G., Yee, H.K.C., Lin, H., Morris, S.L., Hall, P.B., Patton, D.R., Sawicki, M., & Wirth, G.D. 2001a, *ApJ*, 548, L5  
 Hoekstra, H. 2001, *A&A*, 370, 743  
 Hoekstra, H., Yee, H.K.C., & Gladders, M.D. 2001b, *ApJ*, 558, L11  
 Hu, W. 1999, *ApJ*, 522, L21  
 Hu, W. & Tegmark, M. 1999, *ApJ*, 514, L65  
 Jain, B., & Seljak, U. 1997, *ApJ*, 484, 560  
 Kaiser, N. 1992, *ApJ*, 388, 272  
 Kaiser, N., Squires, G., & Broadhurst, T. 1995, *ApJ*, 449, 460  
 Kaiser, N., Wilson, G., & Luppino, G.A. 2000, *ApJL*, submitted, astro-ph/0003338  
 Kuijken, K. 1999, *A&A*, 352, 355  
 Luppino, G.A., & Kaiser, N. 1997, *ApJ*, 475, 20  
 Mackey, J., White, M., & Kamionkowski, M. 2001, *MNRAS*, submitted, astro-ph/0106364  
 Maoli, R., Van Waerbeke, L., Mellier, Y., Schneider, P. Jain, B., Bernardeau, F., Erben, T. & Fort, B. 2001, *A&A*, 368, 766  
 Mellier, Y. 1999, *ARA&A*, 37, 127  
 Peacock, J.A., & Dodds, S.J. 1996, *MNRAS*, 280, L19  
 Refregier, A. 2001, submitted to *MNRAS*, astro-ph/0105178  
 Schneider, P. 1998, *ApJ*, 498, 43  
 Schneider, P., van Waerbeke, L., Jain, B., & Kruse, G. 1998, *MNRAS*, 296, 873  
 Tyson, J.A., Wenk, R.A., & Valdes, F. 1990, *ApJ*, 349, L1  
 Van Waerbeke, L., et al. 2000, *A&A*, 358, 30  
 Van Waerbeke, L., et al. 2001, *A&A*, 374, 757  
 Wittman, D.M., Tyson, J.A., Kirkman, D., Dell'Antonio, I., & Bernstein, G. 2000, *Nature*, 405, 143